

Ring Nebula and Bipolar Outflows Associated with the B1.5 Supergiant Sher #25 in NGC 3603¹

Wolfgang Brandner², Eva K. Grebel^{2,3}, You-Hua Chu^{3,5}, Kerstin Weis^{3,4,5}

²*Astronomisches Institut der Universität Würzburg, Am Hubland, D-97074 Würzburg, Germany*

³*University of Illinois at Urbana-Champaign, Department of Astronomy, 1002 West Green Street, Urbana, IL 61801, USA*

⁴*Institut für Theoretische Astrophysik, Tiergartenstr. 15, D-69121 Heidelberg, Germany*

⁵*Visiting astronomer, Cerro Tololo Inter-American Observatory, NOAO, which are operated by AURA, Inc., under contract with the NSF*

ABSTRACT

We have identified a ring-shaped emission-line nebula and a possible bipolar outflow centered on the B1.5 supergiant Sher #25 in the Galactic giant HII region NGC 3603 (distance 6 kpc). The clumpy ring around Sher #25 appears to be tilted by 64° against the plane of the sky. Its semi-major axis (position angle $\approx 165^\circ$) is $6''.9$ long, which corresponds to a ring diameter of 0.4 pc. The bipolar outflow filaments, presumably located above and below the ring plane on either side of Sher #25, show a separation of ≈ 0.5 pc from the central star.

High-resolution spectra show that the ring has a systemic velocity of $V_{\text{LSR}} = +19$ km s⁻¹ and a de-projected expansion velocity of 20 km s⁻¹, and that one of the bipolar filaments has an outflow speed of ~ 83 km s⁻¹. The spectra also show high [NII]/H α ratio, suggestive of strong N enrichment. Sher #25 must be an evolved blue supergiant (BSG) past the red supergiant (RSG) stage. We find that the ratio of equatorial to polar mass-loss rate during the red supergiant phase was ≈ 16 . We discuss the results in the framework of RSG–BSG wind evolutionary models.

We compare Sher #25 to the progenitor of SN 1987 A, which it resembles in many aspects.

Subject headings: Stars: evolution, individual (Sher #25), mass-loss, and supergiants – supernovae: individual (SN 1987 A) – ISM: individual (NGC 3603).

¹Based on observations obtained at the European Southern Observatory, La Silla

1. The Blue Supergiant Sher #25 in NGC 3603

Sher #25 (Sher 1965) is a B1.5Iab supergiant (Mofat 1983) similar to Sk-69202, the progenitor of SN1987A. Sher #25 has a visual magnitude of $V \approx 12^m2-12^m3$ (e.g., van den Bergh 1978). It is located at $\approx 20''$ north of HD 97950, the core of the ≈ 4 Myr old cluster at the center of the Galactic giant HII region NGC 3603 at a distance of 6–7 kpc (Clayton 1986; Melnick et al. 1989). Based on UBV CCD photometry of Sher #25 Melnick et al. derived a visual extinction $A_V \approx 5^m$ and a distance modulus consistent with Sher #25 being associated with NGC 3603.

In a recent search for emission-line objects in NGC 3603 (Brandner et al. 1997), we found a clumpy ring and a bipolar nebula around Sher #25. This ring is similar to that around SN1987A in both size and morphology. Follow-up spectroscopy shows N enrichment in the nebula around Sher #25, suggesting that Sher #25 is at a similar evolutionary stage as Sk-69202. In this letter, we report our observations (§2), discuss the physical structure of the nebula around Sher #25 (§3) and the evidence for Sher #25 being associated with NGC 3603 (§4), and compare it to SN1987A (§5).

2. Observations

H α and R images of an $8' \times 8'$ field centered on NGC 3603 were obtained at the ESO New Technology Telescope (NTT) on 1995 February 8 with the red arm of the ESO Multi-Mode Instrument and a 2k Tek CCD (ESO #36). We used a narrow-band H α filter ($\Delta\lambda=1.8$ nm) and a broadband R filter for continuum subtraction. Photometric VRI observations and an H α + [NII] image ($\Delta\lambda=6.2$ nm) were obtained on 1995 March 2 with the CCD camera at the Danish 1.54m telescope. The H α + [NII] image of the central cluster in NGC 3603 and its surroundings is displayed in Figure 5. Figure 1 shows a continuum-subtracted H α NTT-image centered on Sher #25. The residuals (bright features) are due to charge bleeding as the brightest stars were saturated in the R image. Figure 2 shows the location of the blue supergiant Sher #25 above and to the red of the main sequence turn-off. The stars well above the main-sequence are (blended) Wolf-Rayet and early type O stars located in the very center of the cluster.

Long-slit echelle spectra of the eastern cap and the

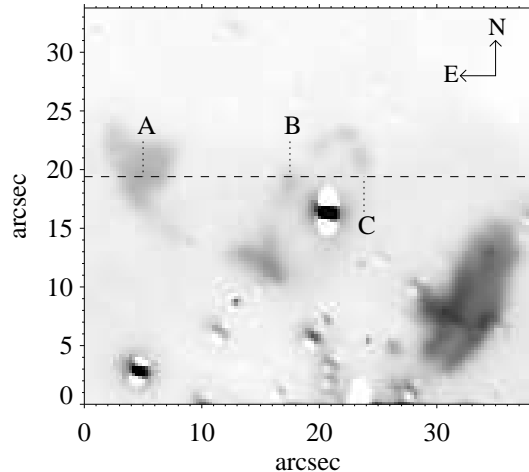


Fig. 1.— Continuum-subtracted H α image (NTT / EMMI, exposure time 10 min, seeing $1''$) of Sher #25 ($\alpha_{2000} = 11^h15^m7.8^s$, $\delta_{2000} = -61^\circ15'17''$). The tilted ring around the blue supergiant as well as the bipolar filaments located to the northeast and southwest of Sher #25 are visible. The position of the slit is indicated by a dashed line.

ring were obtained on 1996 January 10 at the CTIO 4m telescope. The echelle spectrograph was equipped with a 2k Tek CCD. The slit orientation was east-west (dashed line in Figure 1) and the slit width was $1''.6$. We adopted rest wavelengths in air of 654.81 nm and 658.36 nm for the two forbidden [NII] lines $^3P_1-^1D_2$ and $^3P_2-^1D_2$ (e.g., Moore 1959). Relative velocities are accurate to about 0.2 km s^{-1} . The absolute calibration with respect to the local standard of rest (LSR) has an uncertainty of about $2-4 \text{ km s}^{-1}$. Figure 3 shows the 2D spectra in the region of the H α and [NII] lines. At the position where the slit intersects the ring the two distinct velocity components are clearly visible.

3. Inner Ring and Outflow Filaments around Sher #25

A tilted ring around Sher #25 can be clearly seen in Figures 5 and 1. The semi-major and semi-minor axes are $6''.9$ and $3''.05$, respectively. Assuming a circular ring geometry, we derive an inclination angle of 64° with respect to the sky plane along the position angle $\approx 165^\circ$. The linear diameter of the ring is 0.4 pc, for a distance of 6 kpc. The relative velocity difference between the two ring components intersected

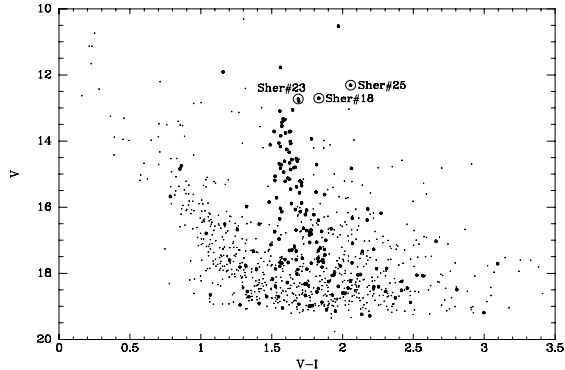


Fig. 2.— Color-magnitude diagram for NGC 3603 and the surrounding field. Stars within the central $70'' \times 70''$ ($2\text{pc} \times 2\text{pc}$) around the cluster center are marked by fat dots, the field (foreground) star population is marked by thin dots. The three blue supergiants are highlighted by an open ring.

by the slit is 32 km s^{-1} (cf. Figure 4). Taking projection effects into account, we derive a de-projected expansion velocity of 20 km s^{-1} for the ring and a systemic velocity of $v_{\text{LSR}} = +19 \text{ km s}^{-1}$. This value agrees well with radial velocities of molecular cloud cores south of NGC 3603 ($+12 \text{ km s}^{-1}$ to $+16 \text{ km s}^{-1}$, Nürnberger, priv. comm.) and supports Sher #25’s association with NGC 3603.

Bipolar filaments to the northeast and to the southwest of Sher #25 are also clearly visible in Figures 5 and 1. The northeast filament is not resolved into substructures. It is blue-shifted by 36.2 km s^{-1} from the systemic velocity, indicating an outflow nature. The southwestern filament shows a complex structure with two apparent shock fronts. Lacking kinematic information, we cannot determine whether the southwestern filament is part of a larger 3D structure, i.e., something hourglass-like. Nevertheless, it is very likely that these bipolar filaments are physically produced by a bipolar outflow. If the bipolar filaments of Sher #25 are located along an axis perpendicular to the plane defined by the ring, their physical separation from Sher #25 is about 0.5 pc ($15''/\cos 26^\circ$ at 6 kpc). The de-projected expansion velocity of the northeastern filament is $\approx 83 \text{ km s}^{-1}$.

The echelle spectra of the ring and the northeast outflow filament show a high $[\text{NII}]/\text{H}\alpha$ ratio, compared to the background HII region (see Table 1 and Figure 4). Low-resolution spectra of the north-

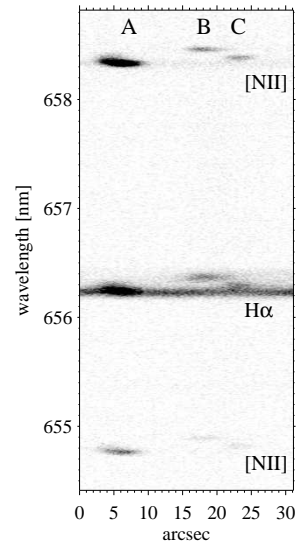


Fig. 3.— 2D high-resolution spectra of stellar ejecta associated with Sher #25. Two distinct velocity components where the slit intercepts the ring (B&C) are visible in $\text{H}\alpha$ and $[\text{NII}]$.

eastern outflow filament indicate $T_{\text{eff}} \approx 7000 \pm 1000 \text{ K}$ and $\log N_e \approx 9.8 \pm 0.3 \text{ m}^{-3}$. In a $[\text{OIII}]/\text{H}\beta$ vs. $[\text{NII}]/\text{H}\alpha$ diagram, the north-eastern outflow filament is situated clearly outside the location of HII regions or supernova remnants (Brandner et al. 1997). Thus, the high $[\text{NII}]/\text{H}\alpha$ ratio is caused by an enhanced N abundance, indicating that at least the bipolar filaments around Sher #25 consist of stellar material enriched by the CNO cycle. Therefore, Sher #25 very likely is an evolved post-red supergiant.

Given the evolutionary stage of Sher #25, the surrounding nebula may be explained in the framework of interaction between red supergiant (RSG) wind and blue supergiant (BSG) wind. A 2D ring-like structure (as opposed to 3D shells) can be produced if the density of the RSG wind is a strong function of polar angle, peaking along the equatorial plane and decreasing toward the poles (Blondin & Lundqvist 1993; Martin & Arnett 1995). A ring develops as the fast BSG wind sweeps up the dense RSG wind material. At the same time the density gradient in the RSG wind allows the fast BSG wind to expand more easily in polar directions. This process might lead to an hourglass-shaped emission nebula as has been observed in the young planetary nebula MyCn18 (Sahai et al. 1995). The clumpy structure of the ring (see Figure 1) very likely originates in Rayleigh-Taylor in-

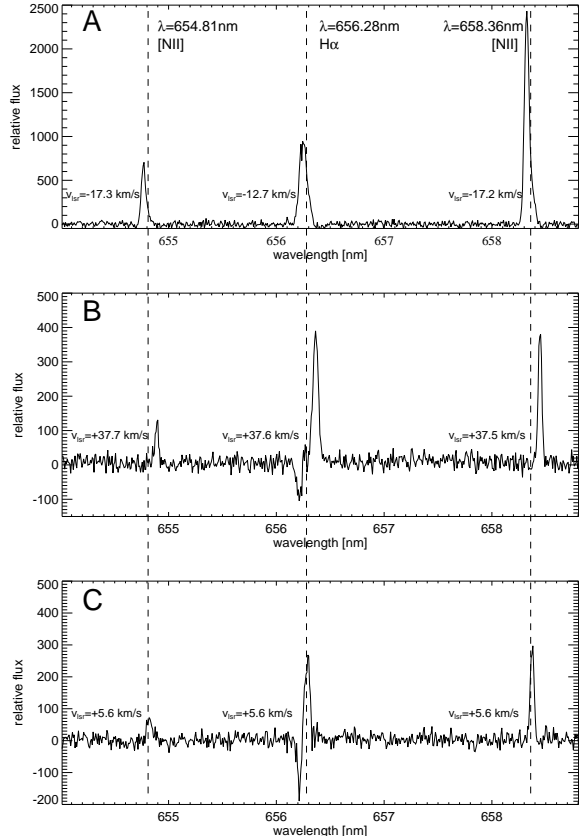


Fig. 4.— Radial velocities of H α and [NII] emission lines in the outflow filament A and the two ring fragments B and C with respect to the local standard of rest. The dashed lines indicate the rest wavelengths of the emission lines. The spectra are background subtracted by linear interpolation between the nebular emission east and west of the individual knots. The absorption feature on the blue side of the H α line at position B and C is due to imperfect background subtraction.

stabilities at the interface between the swept-up slow RSG wind and the fast BSG wind.

The expansion velocities and physical dimensions yield a dynamical age of ≈ 9000 yr for the ring and ≈ 6000 yr for the polar outflows. Applying a self-similarity solution for the interaction regions of colliding winds (e.g., Chevalier & Imamura 1983) we can carry out a crude analysis of the observed velocities. In the following we assume constant mass loss rates and constant wind velocities for the slow wind and the fast wind, a stalled shock (pressure equilibrium) in a spherical symmetric fast wind, and an adiabatic (non-radiative) shock. The shock then expands with

a velocity of

$$v_{\text{shock}} \approx \left(\frac{\dot{M}_{\text{fw}} v_{\text{fw}} v_{\text{sw}}}{\dot{M}_{\text{sw}}} \right)^{1/2}$$

where \dot{M}_{fw} , \dot{M}_{sw} , v_{fw} , and v_{sw} are mass-loss rate and wind velocity of the fast wind (fw) and the slow wind (sw), respectively.

If the fast wind is isotropic and does not show any variation in density as a function of polar angle, then the ratio of the expansion velocity of the polar outflow (83 km s^{-1}) to that of the ring (20 km s^{-1}) gives us directly the ratio of RSG mass loss in both directions: $\dot{M}_{\text{sw}}(0^\circ)/\dot{M}_{\text{sw}}(90^\circ) \approx 16:1$. This is in reasonable agreement with the ratios of 20:1 and 10:1 computed for the progenitor of SN 1987 A by Blondin & Lundqvist (1993) and by Martin & Arnett (1995), respectively. Assuming a fast wind velocity of 800 km s^{-1} , a slow wind velocity of 50 km s^{-1} , and a ratio of the slow wind and fast wind mass-loss rates along the stellar equator of 90:1 (6:1 in polar direction) one is able to reproduce the observed shock velocities in the framework of this very simplified model.

The center of the inner ring does not coincide with the position of Sher #25 (offset $1''$ to $2''$). This may be due to a movement of Sher #25 relative to the surrounding ISM. Martin & Arnett (1995) pointed out that such a movement would produce asymmetric polar outflow structures, which in turn might explain the different appearance of the northeastern and southwestern polar outflow filaments of Sher #25. However, the interpretation of the filaments may be complicated by Sher #25's apparent location at the edge of a wind-blown cavity excavated by the central cluster of NGC 3603 (Figure 5). This cavity has a diameter of 2 pc, a dynamical age of 10^4 yr (Clayton 1986) and may have been created by the onset of the Wolf-Rayet phase of the three central stars of NGC 3603 (Drissen et al. 1995).

4. Sher #25 and its relation to NGC 3603

What evidence do we have that Sher #25 is indeed a member of the giant HII region NGC 3603? Firstly, as discussed above, the systemic velocity of the ring is in good agreement with the line-of-sight velocities of the cloud cores south of HD 97950. Secondly, Sher #25 is not the only BSG in the NGC 3603 region. Spectroscopy by Moffat (1983) revealed two other BSG in the vicinity of the cluster core (cf. Figure 5). The locations of Sher #18 (O6If) and Sher

#23 (O9.5Iab) are also indicated in our V vs. V-I CMD (Figure 2). The apparent lack of BSGs with similar reddening among the “field stars” (thin dots in Figure 2) adds additional weight to the assumption that Sher #25 is associated with NGC 3603.

Could Sher #25 then have been born at the same time as the massive central stars of the cluster? This would require that Sher #25 originally had been at least as massive as these central stars and has gone through a violent Luminous Blue Variable (LBV) phase with a total mass-loss of more than 50% of its initial mass (i.e., $\dot{M} \geq 25 M_{\odot}$) before it became a BSG. Indeed, kinematical age, expansion velocity, and abundances of Sher #25’s nebula are comparable to those of the AG Car nebula (cf. e.g., Leitherer et al. 1994). With $M_{\text{bol}} \approx -9^m1$, Sher #25’s luminosity is in the range of luminosities observed in other LBVs. Thus, an LBV evolutionary scenario for Sher #25 and its circumstellar surrounding cannot be entirely excluded.

The simultaneous presence of BSGs and stars of MK type O3V (cf. Drissen et al. 1995) requires at least two distinct episodes of star formation in NGC 3603 separated by ≈ 10 Myr. Moffat (1983) and Melnick et al. (1989) already suggested that star formation in NGC 3603 might not have been coeval. The starburst in the dense cluster of NGC 3603 might have been initiated by the first generation of massive stars through their interaction with a dense cloud core. Subsequently, this cloud core developed into the present-day starburst. A similar evolutionary scenario has been suggested by Hyland et al. (1992) in order to explain the starburst in the 30 Dor region.

5. Sher #25 and SN 1987 A

Sher #25’s circumstellar nebula resembles that of SN 1987 A in many aspects. Both objects have an equatorial ring and bipolar nebulae, and show high $[\text{NII}]/\text{H}\alpha$ ratios, indicating an enhanced N abundance. The N enrichment indicates that the rings and the bipolar nebulae consist of mass lost from the progenitor at an earlier evolutionary stage and swept up by the fast BSG wind. Surface enrichment with material processed by the CNO cycle typically occurs at the very end of the RSG phase within the last 10^4 yr of RSG evolution.

Yet, differences exist. As shown in Table 1, the expansion velocities and $[\text{NII}]/\text{H}\alpha$ ratios are different. The $[\text{NII}]/\text{H}\alpha$ ratio of the nebula around Sher #25 is

lower than the ratio observed in the outer northern ring around SN 1987 A despite the lower N abundance in the LMC. Furthermore, Sher #25 exhibits a higher $[\text{NII}]/\text{H}\alpha$ ratio in the bipolar nebulae than in the ring, while SN 1987 A shows an opposite trend.

The similarities between the nebulae seem to suggest that Sher #25 is at a similar evolutionary stage as the late progenitor of SN 1987 A, Sk-69 202. However, the differences between the nebulae imply that the evolutionary history differs. This may be due to the abundance differences between the young population in the LMC and in the Milky Way, and to mass differences between the two stars.

Sher #25 appears to have been in a rather stable BSG evolutionary phase during the past decades covered by photometric measurements. Its photometry (Table 2) is quite inhomogeneous owing to the variety of different measurement techniques used, crowding problems, and spatial variations in the strength of the nebular background emission. The overall amplitude of variation in V is less than 0^m25 within the last 35 yr, and less than 0^m1 over the last 25 yr. The progenitor of SN 1987 A did not stand out as a variable star, either.

Will Sher #25 explode like Sk-69 202 in the near future? The presence of the ring around Sher #25, the N enrichment in the outflows, and the surface enrichment in metals all suggest that Sher #25 has passed at least once through the RSG phase and is now well within its final BSG phase, which may last a few 10^4 yr in total depending on the initial stellar mass (see Martin & Arnett 1995). Evolutionary models for massive stars, however, still suffer from many unsolved problems, such as the amount of overshooting, semiconvection, mixing, and mass loss, the choice of convection criteria, and metallicity effects (see, e.g., Langer & Maeder 1995). At present, it is premature to predict whether Sher #25 will succeed Sk-69 202 to provide another spectacular supernova in the southern sky soon.

WB acknowledges support by the Deutsche Forschungsgemeinschaft (DFG) under grant Yo 5/16-1. EKG and YHC were partially supported by the NASA grants STI6122.01-94A, NAGW-4519, and NAG 5-3256. EKG acknowledges support by the German Space Agency (DARA) under grant 05 OR 9103 0. We thank our referee Laurent Drissen for helpful comments.

Fig. 5.— $H\alpha+[NII]$ image (Danish 1.54 telescope, exposure time 100 s, seeing $0''.9$) of NGC 3603. The wind-blown cavity around the central cluster is visible. The three blue supergiants in this field are marked. Sher #25 is located at the northern edge of the cavity.

REFERENCES

- Blondin, J.M., & Lundqvist, P. 1993, ApJ, 405, 337
- Brandner, W., Dottori, H., Grebel, E.K., et al. 1997, A&A, *Stellar and non-stellar emission line objects in NGC 3603*, to be submitted
- Chevalier, R.A., & Imamura, J.N. 1983, ApJ, 270, 554
- Clayton, C. 1986, MNRAS, 219, 895
- Drissen, L., Moffat, A.F.J., Walborn, N.R., & Shara, M.M. 1995, AJ, 110, 2235
- Hyland A.R., Straw S., Jones T.J., Gatley I. 1992 MNRAS 257, 391
- Jakobsen, P., Albrecht, R., Barbieri, C., et al. 1991, ApJ, 369, L63
- Langer, N., & Maeder, A. 1995, A&A, 295, 685
- Leitherer C., Allen R., Altner B. et al. 1994 ApJ 428, 292
- Martin, C.L., & Arnett, D. 1995, ApJ, 447, 378
- Melnick, J., Tapia, M., & Terlevich, R. 1989, A&A, 213, 89
- Moffat, A.F.J. 1974, A&A, 35, 315
- Moffat, A.F.J. 1983, A&A, 124, 273
- Moffat, A.F.J., Drissen L., & Shara M.M. 1994 ApJ 436, 183
- Moore, C.E. 1959, *A Multiplet Table of Astrophysical Interest*, United States Department of Commerce, Washington, D.C.
- Panagia, N., Gilmozzi, R., Macchetto, F. et al. 1991, ApJ, 380, L23
- Panagia, N., Scuderi, S., Gilmozzi, R., et al. 1996, ApJ, 459, L17
- Plait, P.C., Lundqvist, P., Chevalier, R.A., & Kirshner, R.P. 1995, ApJ, 439, 730
- Sahai, R., Trauger, J.T., & Evans, R.W. 1995, BAAS, 27, 1344
- Sher, D. 1965, MNRAS, 129, 237
- van den Bergh, S. 1978, A&A, 63, 275

This 2-column preprint was prepared with the AAS L^AT_EX macros v4.0.

TABLE 1

PHYSICAL PROPERTIES OF THE CIRCUMSTELLAR ENVIRONMENT OF SHER #25 AND SK-69°202 / SN 1987 A.
WE REPORT THE RATIO OF $[\text{NII}]654.8+658.3/\text{H}\alpha$.

	Sher#25	Sk-69°202 / SN 1987 A
$d_{\text{(inner)ring}}$	0.4 pc	0.4 pc ^a
$v_{\text{(inner)ring}}$	20 km s ⁻¹	10 km s ^{-1b}
v_{poles}	83 km s ⁻¹	
$([\text{NII}]/\text{H}\alpha)_{\text{ring}}$	0.9–1.2 : 1	4.2 : 1 ^c
$([\text{NII}]/\text{H}\alpha)_{\text{poles}}$	2.1 : 1	2.5 : 1 ^c
$([\text{NII}]/\text{H}\alpha)_{\text{background}}$	0.15 : 1	0.09 : 1 ^d

^aPanagia et al. 1991, Plait et al. 1995

^bJakobsen et al. 1991

^cPanagia et al. 1996

^dChu, unpublished

TABLE 2

PHOTOMETRIC OBSERVATIONS OF SHER #25.

Reference	date	V	B-V	U-B
Sher (1965)	≈1962	12 ^m 07	+1 ^m 59	+0 ^m 19
^a van den Bergh (1978)		12 ^m 08	+1 ^m 59	+0 ^m 19
Moffat (1974)	≈1972	12 ^m 27	+1 ^m 36	+0 ^m 10
^a van den Bergh (1978)		12 ^m 38	+1 ^m 40	+0 ^m 29
van den Bergh (1978)	1976/77	12 ^m 28	+1 ^m 38	+0 ^m 25
Melnick et al. (1989)	1985 Feb.	12 ^m 20	+1 ^m 42	+0 ^m 13
Moffat et al. (1994)	1991 Feb.	—	— ^b	—
This paper	1995 March 2	12 ^m 31	c	—

^aapplying photometric transformations as derived by van den Bergh (1978)

^bUsing HST/PC1 Moffat et al. (1994) measured B=13^m50.

^cVRI measurements: V-R=+1^m03, R-I=+1^m03